Pergamon

Cement and Concrete Research, Vol. 28, No. 11, pp. 1605–1619, 1998

0008-8846/98 $19.00 + .00

PII S0008-8846(98)00141-0

CHARACTERIZATION AND COMPARATIVE STUDY OF COAL COMBUSTION RESIDUES FROM A PRIMARY AND ADDITIONAL FLUE GAS SECONDARY DESULFURIZATION PROCESS

S. Gomes,[1]* M. François,* C. Pellissier,† and O. Evrard*

*Laboratoire de Chimie du Solide Minéral, UMR CNRS 7555, Université Henri Poincaré, Nancy, BP 239, 54506 Vandoeuvre Cedex, France

†EDF-CNET, les Collines de l'Arche, Cedex 24-92057 Paris la Défense, France

(Received January 4, 1998; in final form August 17, 1998)

ABSTRACT

An extensive characterization and comparative study was done on two flue gas desulfurization (FGD) residues derived from the same coal. LR residues (originated from Loire/Rhône in the south of Lyon, France) are obtained after a "primary desulfurization" process (SO_2 is trapped by reaction with CaO at a temperature of about 1100°C), and LM residues (originating from La Maxe, near Metz in the east of France) are obtained after an additional "secondary desulfurization" process (SO_2 is removed further by reaction with $Ca(OH)_2$ at a temperature of about 120°C). Various and complementary investigation methods were used to determine their chemical, physical, and mineralogical properties: x-ray fluorescence and diffraction, scanning electron microscopy, differential scanning calorimetry, thermogravimetry analysis, granulometric distribution, pycnometric density, BET specific surface area and pH, conductivity measurements, and chemical analysis of their insoluble fraction. The FGD residues contain basically two main components: a silico-aluminous fly ash part and calcic FGD phases. In the LR residues the two components can be considered as independent, whereas they are linked in the LM residues because chemical reactions have occurred, leading to the formation of silico-calcic gel CSH, hydrated aluminate AFm, and AFt phases. *© 1998 Elsevier Science Ltd*

Introduction

Over the last few decades, environmental legislation has forced electricity producers using coal combustion in power plants to equip their installations with flue gas desulfurization (FGD) systems to reduce the quantities of sulfur dioxide emitted into the atmosphere. Therefore, since 1992 the Loire/Rhône's (LR, situated in the south of Lyon, France) and La Maxe's (LM, situated in the north of Metz, France) power plants, both belonging to EDF (Electricité de France), have been equipped with what is called a "primary desulfurization"

[1]To whom correspondence should be addressed.

system. It is based on injection of hydrated lime or pulverised limestone, at about 30 m above the heart of the furnace. The LM power plant also is equipped with an additional system, which consists of a "secondary desulfurization" system situated downstream of the boiler. Water and hydrated lime are injected at a temperature of about 120°C. This system is a pilot installation that treats only 7% of the fume.

Both samples studied here originated from the same bituminous coal, which contains about 0.9 wt% of sulfur (ratio Ca:S = 4.5).

Primary desulfurization is based on the following chemical reactions, occurring at a temperature of about 1100°C: limestone decarbonation, $CaCO_3$ $CaO + CO_2$, followed by lime sulfatation, $CaO + SO_2 + ½O_2 \rightarrow CaSO_4$. The desulfurization process is known to be economical, because it can be installed easily on existing plants. The efficiency of "primary desulfurization" is about 50%. The FGD residues collected after this treatment consist of fly ash mixed with FGD phases.

Secondary desulfurization allows desulfurization efficiency to increase to 90% and is based on reactions occurring at a lower temperature ($T \approx 120$°C) than primary desulfurization and in a moist atmosphere. Thus, sulfur dioxide is "trapped" by calcium hydroxide to produce calcium sulphite hemihydrate and gypsum, according to the reactions: $Ca(OH)_2 + SO_2 \rightarrow CaSO_3{\cdot}0.5H_2O + ½\ H_2O$ and $Ca(OH)_2 + SO_2 + ½O_2 + H_2O \rightarrow CaSO_4{\cdot}2H_2O$. The residues ashes collected after this treatment differ because of their high hemihydrate concentration.

Silico-aluminous fly ashes, the usual ash from power plants, but which are not treated by a primary or secondary desulfurization process, long have been extensively used in the civil engineering field. They are used mainly in concrete or clinker extender and in road building. There have been numerous studies of clinker or cement containing up to 60 wt% of silico-aliminous fly ashes (1–5). Mineralogical properties of such ashes are well known (6–17). They contain mullite, α-quartz, magnetite, hematite, and a vitreous phase.

As desulfurization is a relatively new process, only a few studies dealing with primary FGD residues originating from France (18,19) or the United States (20,21) have been published (the equivalent of such residues in the US are called LIMB residues, as they are formed by limestone injection multistage burner technology, or Sorbent injection residues). It is known that primary FGD residues can be considered a blend composed of silico-aluminous fly ashes, lime, calcite, and calcium sulphate and have cementitious properties.

Moreover, to our knowledge, the secondary FGD residues issued from the new experimental process applied only in a pilot installation at La Maxe in France have no foreign equivalent among the various residues issued from the "clean coal technology" reported in the literature. A work concerning silico-sulfited residues, produced in a German power plant, has been published (22). Their utilisation in cements concrete is discussed.

The aim of this work was to study the influence of desulfurization processes (primary and secondary) on the physical, chemical, and mineralogical properties of these residues. The second wet and low temperature process could result in important changes, as it is applied to primary FGD residues already having cementitious properties. For this purpose, two different samples of desulfurization ashes were studied: the LR sample, from Loire/Rhône's power plant, desulfurization with the primary process, and the LM sample, from La Maxe's power plant, desulfured with a primary and an additional secondary process. It is useful to point out that the LM and LR residues are sampled immediately before being conditioned with water to prevent dusting during transportation or storage. Complete characterization of the LR and LM residues was made using various and complementary techniques: x-ray diffraction

TABLE 1
Density and surface specific area in LR and LM samples.

	LR sample	LM sample
Density (g/cm^3)	2.50	2.27
Specific surface area (m^2/g)	3.34	11.88

(XRD), x-ray fluorescence, scanning electron microscopy (SEM) linked with EDS analysis, thermogravimetry (TGA) and differential scanning calorimetry (DSC) for determination of hydrated phases, BET for surface specific area measurements, conductivity measurements, and chemical analysis of the soluble fraction of the residues.

Experimental Procedure and Results

Description of the Samples

The analysed samples have the usual aspect of desulfurization ashes: a grey powder, with white grains of calcite or lime and small black particles of unburned coal. The main difference between the LR and LM samples is the presence in the latter of agglomerates of grains, which can be several millimetres in size. The grains form during the secondary desulfurization process, in which the wet conditions favour hydration reactions among the different components. The granulometric distribution (not shown here) was determined by a laser granulometer (CILAS type). They are not very different: the median diameter of the particles, D_{50}, is 20 and 25 μm in LR and LM samples, respectively.

Physical Properties

The density of the samples was determined by the pycnometric method using decaline (deca-hydronaphthalen, $\rho = 0.8791$ g/cm^3 at 30°C) as reference. Specific area was determined by BET measurements. The results are reported in Table 1. Interestingly, the densities are similar, whereas the surface specific area of LM sample is much higher than that of LR.

X-ray Fluorescence

The chemical composition of the two samples was determined by x-ray fluorescence and is reported in Table 2. The concentration sum of oxides (SiO_2, Al_2O_3, and Fe_2O_3) has a value of 34.7 wt% and 49.4 wt% in the LR and LM fly ashes, respectively. They differ from class C fly ashes because their high calcium content is due to the desulfurization process and not because of the nature of the source coal. They also differ in having higher SO_3 contents.

The weight loss at 110°C corresponds to free water. It shows that the LM sample contains

TABLE 2
Chemical composition of FGD residues obtained by x-ray Fluorescence.

Elementary oxides	LR sample (wt%)	LM sample (wt%)
SiO_2	18.0	27.3
Al_2O_3	12.2	17.0
Fe_2O_3	4.5	5.1
K_2O	1.7	1.3
MgO	1.8	1.8
Na_2O	0.07	0.15
TiO_2	0.03	0.68
P_2O_5	0.03	0.26
Mn_2O_3	0.07	0.10
Cr_2O_3	0.02	0.02
CaO	41.2	19.4
SO_3	3.8	5.4
Loss on ignition at 975°C	15.4	21.4
Total	98.8	99.9
Loss on ignition at 105–110°C	0.0	5.0
Free lime Leduc* ($CaO + Ca(OH)_2$)	22.9	1.5

* Chemical analysis of free lime (CaO or $Ca(OH)_2$) by Ca^{2+} complexion with a 10% saccharose ($C_{12}H_{22}O_{11}$) solution (1 g of powder in 100 mL of 10% saccharose solution). Titration by HCl acid using phenolphthaleine as an indicator.

5 wt% free water, resulting from the secondary desulfurization, whereas the LR sample contains no measurable free water.

The weight loss at 975°C corresponds to the loss of water chemically bonded in hydrated compounds, CO_2 loss due to decarbonation of the calcite, and the combustion of unburned coal particles. The weight loss value is greater for the LM sample (21.4 wt%) than for the LR sample (15.5 wt%), which indicates that the hydration and or carbonation reactions are most important in the LM sample.

From Table 2, it can be deduced that the calcic FGD phases plus the unburned coal particles represent 60.4 wt% and 46.2 wt% in the LR and LM samples, respectively.

XRD

X-ray powder diffraction patterns were measured on a goniometer with Bragg-Brentano geometry, using filtered CoKα ($\lambda = 1.7889$ Å) radiation. The diffraction patterns were analysed by the DIFFRAC-AT program (23), which included phase identification using the ICDD Powder Diffraction File data base. Powder patterns (selected data range $8° \leq 2\theta \leq 54°$) of the LR and LM samples and of only the silico-aluminous parts of these ashes, which

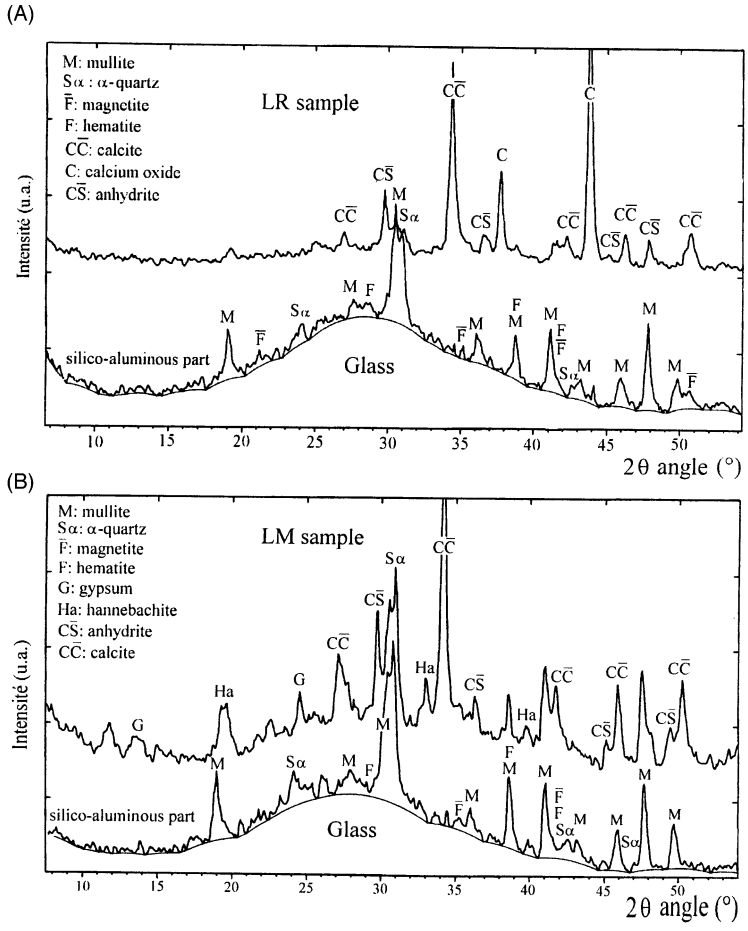

FIG. 1.
X-ray powder pattern (CoKα) (*A*) of LR and (*B*) LM samples.

were separated by washing with the following procedure, are shown in Figure 1. To remove the desulfurization fraction from the FGD residues, 2 g of powder is washed in about 2 L of an aqueous HCl solution (10^{-2} M). The washed powders then are dried and checked by XRD. They did not contain any residual calcic phases. In this experiment, calcite and hannebachite are dissolved completely by acid–basic reaction with the aqueous acid solution. Gypsum and anhydrite, with solubilities of 2.4 and 2.1 g/L (24), can be removed easily.

The silico-aluminous part of the residues clearly shows the hump characteristic of the glass, of which the maximum is situated at 28°. It corresponds to a d value of 3.70 Å, indicating that the amorphous phase is constituted mainly by network-forming oxides SiO_2 and Al_2O_3 (14).

The crystalline phases in the silico-aluminous part of both samples are those usually encountered in class F fly ashes: mullite, a-quartz, magnetite, and hematite. To increase the concentration of the intergrown iron phases, magnetite and hematite, magnetic separation

TABLE 3
XRD parameters and mineralogical composition of the silico-aluminous part of the FGD residues.

Phases	Theta (CoK_α)	hkl	AIR	Wt%
α-SiO_2	15.55	101	1.11	8.7
$Al_6Si_2O_{13}$	19.40	220	0.13	24.7
Fe_3O_4	17.60	220	0.37	4.0
Fe_2O_3	19.40	104	0.40	0.6
Vitreous phase	—	—	—	62.0

with a super permanent magnet in water was done. QXRD analysis by the "full matrix flushing" method previously described (25) was performed, using silicon as an internal standard (reflection (111) at $2\theta = 33.2°$), on a powder diffraction pattern of the whole silico-aluminous part and on the powder containing the iron phases only.

The method used here is based on the determination of analytical intensity ratio (AIR) previously described (26,27). A ratio of intensity of a chosen peak of the analyte to a chosen peak of the internal standard is determined from a reference melt of 50 wt% of pure phase to analyse and 50 wt% of standard. The use of silicon as standard allows one to avoid overlaps with peaks of the analyte. The AIR method can be considered quantitative, as opposed to a semiquantitative method (reference intensity ratio). The AIR of each analysed phase, the corresponding XRD parameters, and the resulting composition are listed in Table 3.

The results for both LR and LM samples led to the following composition, recalculated to the silico-aluminous part, for LR and LM samples: SiO_2 (quartz α) 8.7%, $Al_6Si_2O_{13}$ (mullite) 24.7%, Fe_3O_4 (magnetite) 4.0%, Fe_2O_3 (hematite) 0.6%, and vitreous phase 62.0%.

The remaining crystalline phases largely represent the FGD fraction of the residues. The LR sample contains calcite, calcium oxide, and anhydrite. The LM sample contains calcite, anhydrite, gypsum, and hannebachite (sulfite hemidydrate) but not free lime.

pH and Conductivity

pH and conductivity were measured as various mixtures of FGD residues in demineralised water. The resulting curves for both samples (LR and LM) are shown in Figures 2A and 2B.

The pH curves (Fig. 2A) indicate that the LR sample is significantly more basic. The pH of 12.6 in the LR sample is fixed by the free lime $Ca(OH)_2$. The pH of 10.0 in the LM sample is fixed by $CaCO_3$, $CaSO_4{\cdot}2H_2O$, minor $Ca(OH)_2$ (not seen by XRD but detected by TGA and DSC, as described following), and the pCO_2 in air.

The conductivity of both LR and LM samples increases with the solid:water ratio without reaching a constant value contrarily to the pH curves. This behaviour is dependent on the solubility of the most soluble calcic phases contained in the samples. Their solubility values (24,28) ($CaSO_4$: s = 3.4 g/L at pH 12.6 in LR sample, s = 1.4 g/L at pH 10.0 in LM sample; $CaSO_4{\cdot}2H_2O$: s = 0.9 g/L and $CaCl_2$ = 977.0 g/L at pH 10 in LM sample), and their

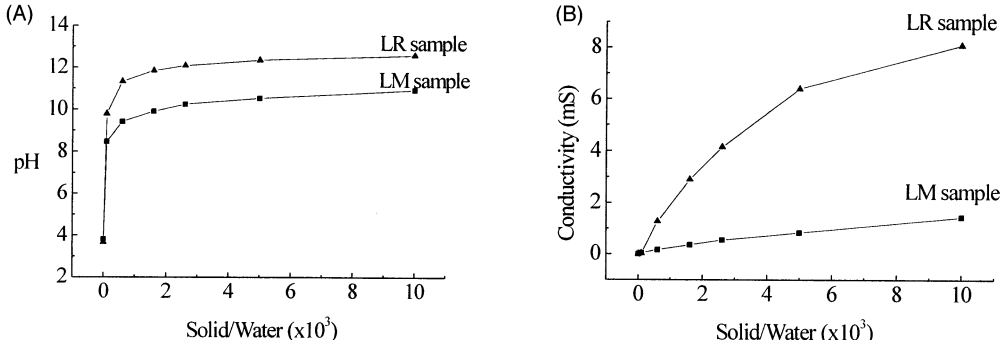

FIG. 2.
pH (*A*) and conductivity (*B*) of the LR and LM fly ashes as a function of the concentration.

concentrations (Table 4) show that even for a solid:water ratio of 1:100, saturation of the solutions is not reached.

The conductivity (Fig. 2B) is significantly higher in the LR than in the LM sample, indicating more significant solubility in the former than in the latter. The soluble fraction of a solution containing 10g/L of fly ashes was dried and weighed. The fraction extracted was

TABLE 4
Mineralogical composition of the LR and LM samples.

Phase	Loire/Rhône's sample (conc. wt%)	Techniques used	La Maxe's sample (conc. wt%)	Techniques used
CaO	21.0	Leduc	0.0	—
$Ca(OH)_2$	2.5	Leduc + TGA	2.0	Leduc
$CaCO_3$	27.9	TGA + XRF	14.3	TGA
$CaSO_4$	6.5 (6.4)	XRF + (chem. anal.)	6.1	XRF + chem. anal.
$CaSO_4{\cdot}2H_2O$	0.0	TGA	3.3	TGA + chem. anal.
$CaSO_3{\cdot}0{\cdot}5H_2O$	0.0	TGA	2.7 (3.0)	TGA + (chem. anal.)
SiO_2	3.2	QXRD	4.7	QXRD
A_3S_2	9.2	QXRD	13.5	QXRD
Fe_3O_4	1.5 (2.4)	QXRD	2.2 (2.6)	QXRD
Fe_2O_3	0.4	QXRD	0.5	QXRD
Coal particles	5.3	TGA	3.3	TGA
Vitreous phase	22.9	QXRD	33.5	QXRD
AFt phases	0.0	—	ε1	TGA, SEM, DSC
CSH	0.0	—	ε2	TGA, SEM, DSC
AFm phases	0.0	—	ε3	TGA, SEM, DSC
$CaCl_2{\cdot}2H_2O$	0.0	—	4	Chem. anal.
			ε1 + ε2 + ε3 = 10.0	

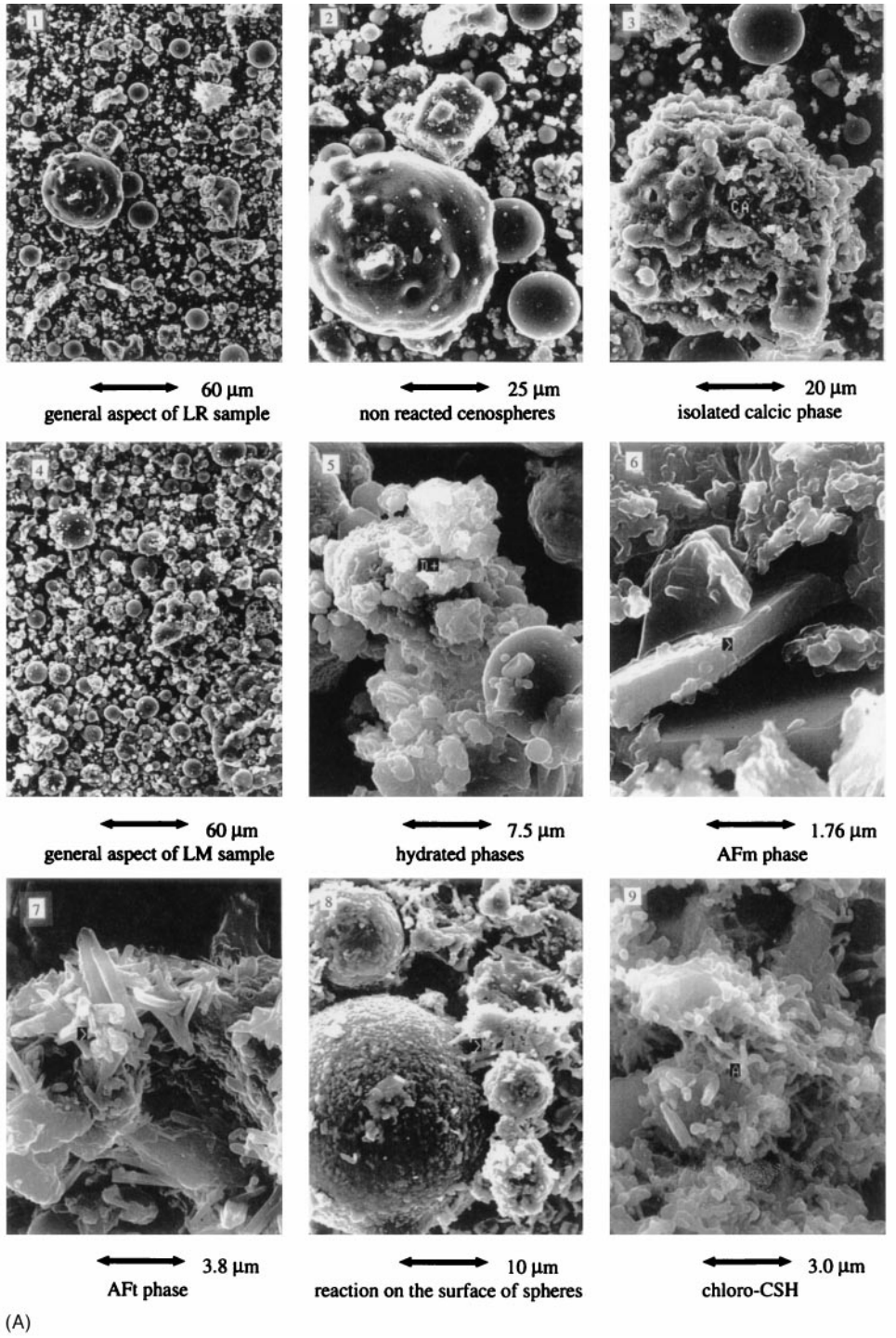

FIG. 3.

SEM photographs (*A*) and corresponding EDS spectra (*B*) of LR (*photos 1–3*) and LM samples (*photos 4–9*).

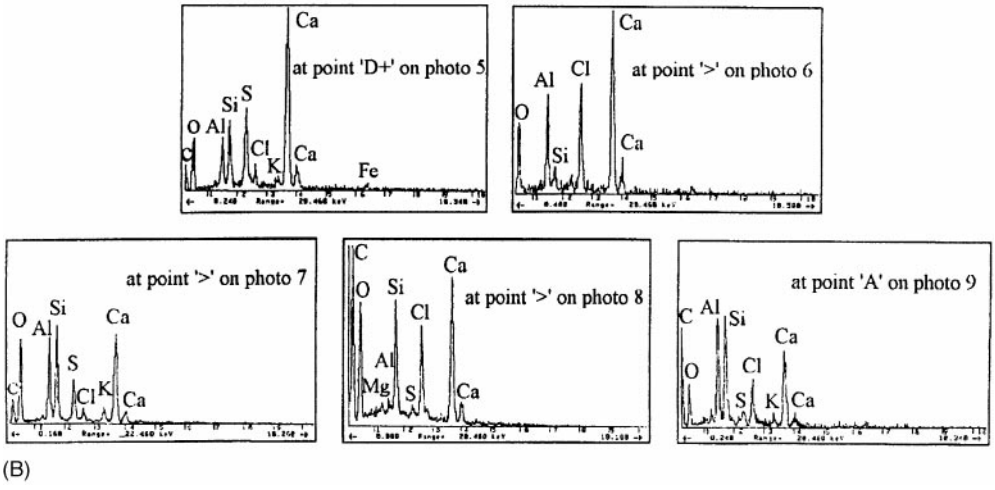

FIG. 3.
Continued

found to be greater in the LR (30 wt%) than in the LM (11 wt%) sample, which is in agreement with the conductivity measurements.

SEM Observations and EDS Analyses

The LR and LM samples were observed by SEM. Photographs at various enlargements and corresponding energy dispersive spectrum (EDS) spectra are shown in Figures 3A and 3B.

General Aspect. Both samples contain characteristic spherules (photo 1, LR sample; photo 4, LM sample) of the silico-aluminous fly ash fraction and the calcic FGD phases. These different components form a blend with some binding in the LM sample but very little binding in the LR sample.

Detailed Aspect

LR Sample. The silico-aluminous fly ash is clearly isolated (spheres on photo 2) from the calcic FGD phases CaO, $CaCO_3$, and $CaSO_4$ (photo 3). This confirms what was seen at lower enlargement. The surface of the spheres are intact (photo 2), indicating that the silico-aluminous fly ash is not attacked during the primary desulfurization process.

LM Sample. All the observations support the premise that the LM sample is a multicomponent system more complicated than the LR one. The silico-aluminous fly ash is embedded in a phase (photo 5) with a geometrical shape that is not very well defined. An EDS analysis on the point marked "D+" shows that this phase contains calcium, silicon, aluminium, sulfur, and, in lower quantity, chlorine and potassium. This could be a chloro-CSH gel containing

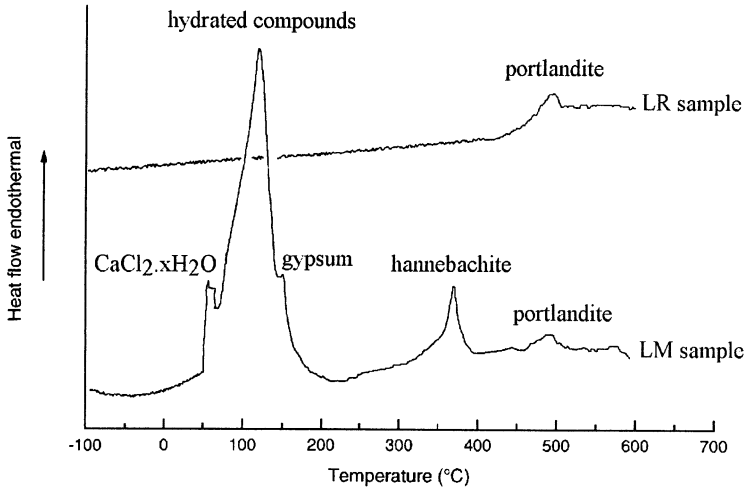

FIG. 4.
DSC curves of the LR and LM fly ashes.

many impurities. Hexagonal-like plates (photo 6) have the characteristic shape of calcium aluminate hydrate crystals. An EDS analysis of such a crystal (at point >) indicates a calcium- and aluminium-rich compound, but also a high chlorine content. This compound could be calcium monochloro-aluminate hydrate (29). Although it is crystallised, it was not detected by XRD because of its apparently low concentration.

Needle-like crystals (photo 7) contain calcium, aluminium, sulfur, and chloride elements. These could be crystals of a chloro-ettringite. Such a compound has been observed in Portland cement when attacked by $CaCl_2$ (29). The spherules are surrounded by a granular film (photo 8) and embedded in an amorphous gel (at point >) containing mainly calcium and silicon, but also a significant quantity of chloride. It could be a "chloro-CSH" similar to that observed by Diamond (30) with a characteristic reticular shape clearly visible in photo 9.

DSC Measurements

DSC over a temperature range of −100°C to +600°C and a heating rate of 10°C/min under a flowing argon atmosphere was used to identify the hydrated phases contained in the samples. The DSC curves are shown in Figure 4 for LR and LM samples.

LR Sample. As expected from the SEM observations and XRD analyses, the only hydrated phase detected in this sample is portlandite, which was not detected by XRD because it is present at too low a quantity. Its dehydration leads to an endothermic peak at 494°C, spread over the temperature range of 470°C to 510°C.

LM Sample. The diagram of the LM sample is much more complicated than the LR one. It must be correlated to a more complex system in LM residue. Five endothermic peaks are detected and their assignments, when it is possible, are reported in the drawing. The sample

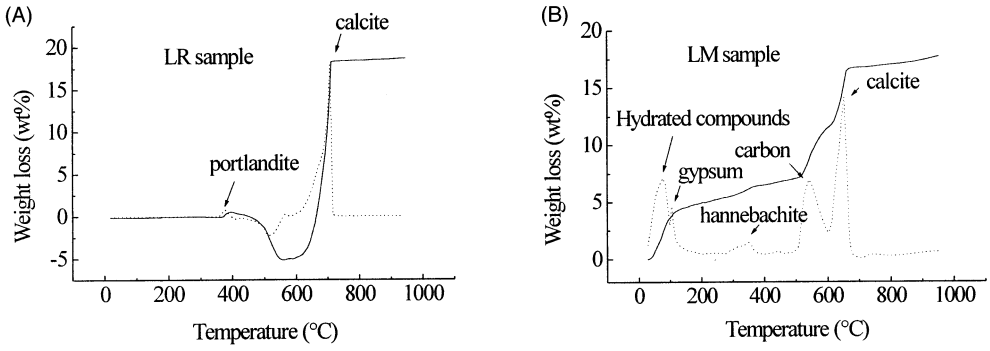

FIG. 5.
TGA curves (*solid lines*) and the derivatives curves (*dashed lines*) of LM and LR fly ashes.

contains gypsum (peak at 140°C), hannebachite (peak at 370°C), and calcium hydroxide (peak at 510°C). It is proposed that the peak at 80°C corresponds to $CaCl_2 \cdot 2H_2O$, and the broad peak at 120°C corresponds to chloro-CSH, AFt (ettringite), and AFm phases called hydrated compounds in the drawing.

Chlorine contained in LM and not in LR residues originates from coal. Whereas chlorine is trapped by water during the low-temperature secondary desulfurization process, apparently it is eliminated into the atmosphere with remaining SO_2 during the high-temperature primary process.

TGA Measurements

TGA was performed between room temperature and 950°C at a heating rate of 0.4°C/min under flowing nitrogen atmosphere and used as a quantification method. The relative weight loss, and the derivative curves, due to the reactions of dehydration and decarbonation are reported as a function of temperature in Figure 5.

LR Sample. The weight loss of 0.6% at 400°C corresponds to the dehydration of 2.5 wt% of $Ca(OH)_2$. The gain weight in the temperature range 400°C to 600°C is noteworthy and needs some explanation. Carbon dioxide is formed by the reaction of the unburned coal particles and the di-oxygen present in very small quantity, even in a normally very pure N_2 atmosphere. It is proposed that the weight gain comes from the carbonation of free-lime CaO by the newly formed CO_2. TGA measurement was stopped at 550°C, and the increased content of calcite and disappearance of CaO were verified by XRD (not shown here). The weight loss of 17.6% between 650°C and 700°C corresponds to the decarbonation of calcite $CaCO_3$. No signal corresponding to combustion of coal particles appears, indicating that the whole carbon fraction was transformed into CO_2, then captured by CaO.

LM Sample. As expected, the curve obtained is more complex than that of the LR sample. Five temperature domains that are emphasised by the derivative curve can be separated.

Between 25°C and 95°C occurs the elimination of slightly bonded water from hydrated

compounds (AFt ettringite, AFm phases, and CSH: see DSC). Between 95°C and 120°C the dehydration of gypsum occurs. The observed weight loss of 0.7% corresponds to dehydration of 3.3 wt% of gypsum.

The weight loss observed between 320°C and 670°C also leads to some quantitative results. The weight loss of 0.19% over the temperature range 320°C to 380°C corresponds to the dehydration of 2.7% of calcium sulfite hemihydrate, and those observed in the temperature range 500°C to 670°C to the decarbonation of 14.3 wt% of calcite and to the elimination of 3.3 wt% of "nonburned particles."

Chemical Analyses of Anions

Sulfate and sulfite concentrations were determined by gravimetry. The method consists of precipitation of sulfate ions with Ba^{2+} ($BaCl_2$) into $BaSO_4$, which then was dried and weighed. Determination of the sulfite concentration needed an additional step: oxidization of the sulfite into sulfate by hydrogen peroxide. Then, the total sulfur species, sulfate, and sulfite can be determined. The sulfite concentration was determined by difference. The result was that the LR ashes contain 6.4 wt% of $CaSO_4$. The LM ashes contained 3 wt% of sulfite ($CaSO_3 \cdot 0.5H_2O$), in agreement with the value of 2.7 wt% obtained by TGA, and 8.7 wt% of sulfate ($CaSO_4$ and $CaSO_4 \cdot 2H_2O$).

The quantity of chloride was determined by precipitation of AgCl by addition of $AgNO_3$ (10^{-1}M). The equivalent point is determined by potentiometry at current zero on a silver electrode. Before the equivalent point, the measured potential is of the $AgCl_{\downarrow}/Ag_{\downarrow}$ system. After the equivalent point, when there is no chloride in solution, the potential is that of the $Ag^{+}/Ag_{\downarrow}$ system. Thus, based on the assumption that the chlorides are contained totally in the calcium chloride hydrated compound, it is determined that the LM sample contains less than 4 wt% of $CaCl_2 \cdot 2H_2O$.

No chloride was detected in the LR sample.

Mineralogical Composition

Earlier quantitative measurements, QXRD, x-ray fluorescence, TGA, and chemical analysis, led to the mineralogical composition of both samples summarised in Table 4. LR sample contains 63 wt% of calcic FGD phases (which includes some amount of unburned coal particles). This value, close to that deduced by x-ray fluorescence results (61 wt%), shows that CaO, $Ca(OH)_2$, $CaCO_3$, and $CaSO_4$ are the only calcic phases present in this sample.

The calcic FGD phases in the LM sample ($Ca(OH)_2$, $CaCO_3$, $CaSO_4$, $CaSO_4 \cdot 2H_2O$, $CaSO_3 \cdot 0.5H_2O$, and $CaCl_2 \cdot 2H_2O$) plus the unburned carbon sum to only 36 wt%, whereas the value estimated by x-ray fluorescence was 46 wt%. The difference of 10 wt% represents the hydrated compounds, CSH (ε1 wt%), AFt (ε2 wt%), and AFm (ε3 wt%) detected by SEM, TGA, and DSC.

The LM fly ashes, a more complicated system than the LR fly ashes, contained nine different calcic FGD phases, six of which are well quantified.

Discussion

The FGD residues are complex systems. In the LR fly ashes (primary desulfurization), 10 different phases are detected; in the LM (secondary desulfurization), 15 phases were detected.

QXRD analyses with internal standards were used for determining the mineralogical composition of the noncalcic fly ash part of the residue. Indeed, mullite, α-quartz, and iron oxides can be isolated easily by washing out the more soluble calcic phases and give well-defined Bragg peaks. Hematite (present at very low proportion and embedded in magnetite) concentration was determined after isolating the magnetic phase. The QXRD technique used here allows one to deduce the vitreous phase by difference.

TGA analysis was quantitative for calcite ($CaCO_3$), gypsum ($CaSO_4 \cdot 2H_2O$), hannebachite ($CaSO_3 \cdot 0.5H_2O$), free lime ($Ca(OH)_2$), and for nonburned carbon.

Chemical analysis of aqueous solutions allowed determination of the proportion of anhydrite ($CaSO_4$) in LR ashes. The relative proportion of gypsum, hannebachite, and anhydrite in LM ashes was determined by three complementary techniques: x-ray fluorescence, chemical analysis, and TGA.

The Leduc method for determining free lime ($CaO + Ca(OH)_2$) is completed by TGA analysis ($Ca(OH)_2$).

The proportion of $CaCl_2 \cdot 2H_2O$ was determined easily by analysing chlorides in aqueous solution.

Hydrated CSH, AFm, and AFt phases were detected by TGA, DSC, and SEM but are not quantified separately. They represent about 10 wt% of the LM residues.

As shown by the analyses just described, the LM and LR FGD residues are quite different with regard to their physical, chemical, and mineralogical properties. It is very important to understand the influence of the primary and secondary desulfurization process when attempting to use these FGD residues in the civil engineering domain (e.g., building of roads, admixtures to cement), as is the case for the classic silico-aluminous fly ashes.

The highest conductivity and, consequently, the highest solubility were observed in the solutions made with LR sample. These properties vary with the concentration of free lime in the samples (21.0 wt% CaO, 2.5 wt% $Ca(OH)_2$ in LR, and 2.0 wt% in LM samples). The silico-aluminous fraction is not soluble in water. The highest solubility of the LR sample suggests that this sample would have better cementitious properties than the LM one.

The relative proportion of FGD calcic phases containing total SO_2 ($CaSO_4 \cdot 2H_2O$, $CaSO_4$, $CaSO_3 \cdot 0.5H_2O$) represents 10.3 wt% and 26.3 wt% of the calcic part (which also includes CaO, $Ca(OH)_2$, $CaCO_3$) in the LR and LM residues, respectively. This shows clearly the efficiency of the secondary desulfurization.

The concentration of $CaCO_3$ in the "calcic part" is high in both samples, 44.3 wt% and 31.1 wt% in the LR and LM sample, respectively. It probably means that the added pulverized limestone was not decarbonated completely during the primary desulfurization process, and the added free lime $Ca(OH)_2$ used in the secondary desulfurization process was carbonated by CO_2 contained in the fume.

The free lime concentration is relatively high in the LR residues (37 wt% of the calcic phases), whereas it is much lower in LM fly ashes (3.3 wt% of the calcic phases). Therefore, the LR residue could give rise to pozzolanic reactions more readily than the LM sample. The LR residue should have characteristics of hydraulic material.

The secondary desulfurization process leads to the formation of hydrated compounds

usually encountered in cement paste (CSH, AFm, and AFt phases). They are present in the LM sample at a proportion of 10 wt%, showing that hydration reactions have started during this secondary process. Hydration reactions lead to partial hardening phenomena, as clearly seen by the formation of conglomerates. The silicate contained in the vitreous phase of the ash is attacked by CaO leading to the CSH formation, and the aluminate readily forms AFm and AFt with CaO and the sulfate/sulfite phases.

The chloride detected in the LM but not in the LR sample is far from insignificant. The chlorides originate from the coal and are trapped by water during the secondary desulfurization process, but are carried off in the flue gas when only the primary one is applied. The trapped quantity of chloride is high enough (4 wt% of $CaCl_2 \cdot 2H_2O$) to induce problems, and one must be prudent when attempting to use such LM residues as extender in cement pastes.

The difference of the specific surface area, significantly higher in the LM than in the LR sample, can be explained by the two following reasons. First, the CSH gel contained in LM residues has a complicated morphology and, consequently, a higher surface than a crystallised phase. But it probably is not the main reason, because CSH is not present in high quantity. Second, the vitreous phase of the silico-aluminous fly ash was attacked by pozzolanic reactions, inducing changes and increasing of the surface of the sphere, as shown by SEM photographs. That could be the main reason for the increase of specific surface area in LM residues compared to the LR residues.

Conclusion

We showed that the FGD residues from a primary desulfurization process and the residues from an additional secondary desulfurization process have different physical, chemical, and mineralogical properties. The changes observed in the LM residues compared to the LR residues are well explained by the reactions occurring during the secondary desulfurization process, mainly, the pozzolanic reactions, leading to new calcic phases (AFm, AFt, CSH), which involved attack on the vitreous phase in the silico-aluminous fly ash.

Acknowledgments

This study is a part of the contract between University Henri Poincaré from Nancy and EDF (Electricité de France), contract no. MX1502. BET measurements were conducted by E. Sauzeat from the "Laboratoire Environnement et Minéralogie" in Nancy, SEM and microprobe analyses by the "Service commun de Micro-analyse," and transmission electron microscopic analyses by the "Service Commun de Microscopie Electronique en Transmission" from the Faculty of Sciences, Vandoeuvre les Nancy (France). Many thanks to Bastien Saïda for the great care she took in correcting the English.

References

1. T.R. Naik, B.W. Ramme and J.H. Tews, ACI Mater. J. 92, 200 (1995).
2. H.F.W. Taylor, K. Mohan and G.K. Moir, J. Am. Ceram. Soc. 68, 685 (1985).
3. P.K. Mehta, Cem. Concr. Res. 11, 507 (1981).
4. P.K. Mehta and O.E. Gjørv, Cem. Concr. Res. 12, 587 (1982).
5. Y. Halse, P.L. Pratt, J.A. Dalziel and W.A. Gutteridge, Cem. Concr. Res. 14, 491 (1984).
6. M. Regourd, 8th ICCC, Rio de Janeiro, Brazil, Abla Gráfica e Editora, I, pp. 200–229 (1986).

7. F.M. Lea, The Chemistry of Cement Concrete, p. 414, A. Edward, London, 1970.
8. H. Pietersen, A.L.A. Fraay and J. Bijen, Mater. Res. Soc. Symp. Proc. 178, 139 (1990).
9. J.C. Qian, E.E. Lachowski and F.P. Glasser, Mater. Res. Symp. Proc. 113, 45 (1988).
10. M. Venuat, Adjuvants et Traitements, p. 249, M. Venuat, Paris, (1984).
11. J.C. Qian, E.E. Lachowski and F.P. Glasser, Mater. Res. Soc. Symp. Proc. 136, 77 (1989).
12. C.L. Kilgour, K.L. Bergeson and S. Schlorholtz, Mater. Res. Soc. Symp. Proc. 136, 161 (1989).
13. M.M. Alasali and V.M. Malhotra, ACI Mater. J. 88, 159 (1991).
14. S. Diamond, Cem. Concr. Res. 13, 459 (1983).
15. G.J. McCarthy, D.M. Johansen and S.J. Steinwand, Adv. X-ray Anal. 31, 331 (1988).
16. G.J. McCarthy and K.J. Solem, Adv. X-ray Anal. 34, 387 (1991).
17. G.J. McCarthy, Mater. Res. Soc. Symp. Proc. 113, 75 (1988).
18. A. Carles-Gibergues and C. Delsol, Bull. Liaison Labo. P. et Ch. 193, 13 (1994).
19. C. Delsol, Perspectives d'emploi en génie civil des cendres volantes de centrales thermiques équipées de systémes de désulfuration primaire, Thesis, University of Toulouse, France, 1995.
20. G.J. McCarthy and J.K. Solem-Tishmack, Adv Cem Concr, p. 103, American Society of Civil Engineers, New York, New York, 1994.
21. J.K. Solem and G.J. McCarthy, Mater. Res. Soc. Symp. Proc. Series 245, 71 (1992).
22. A. Carles-Gibergues and B. Husson, Annales de l'ITBTP 488, 14 (1990).
23. J. Nusinovici and M.J. Winter, Adv. X-ray Anal. 37, 59 (1994).
24. F.H. Chung, J. Appl. Cryst. 7, 519 (1973).
25. A. Thedchanamoorthy and G.J. McCarthy, Adv. X-ray Anal. 32, 569 (1989).
26. J.A. Bender, J.K. Solem, G.J. McCarthy, M.C. Oseto and J.E. Knell, Adv. X-ray Anal. 36, 343 (1993).
27. R.C. Weast (ed.) Handbook of Chemistry and Physics, 57th edition, Chemical Rubber Publishing Co., Cleveland, Ohio, 1976–1977.
28. S. Papayannakis, Réactivité de l'anhydrite naturelle et sa valorisation en tant que matériau de construction, Thesis, University of Nancy, France, 1991.
29. M. Conjeaud, Mécanisme d'attaque des ciments Portland par $CaCl_2$, M. Murat Ed., pp. 171–181 (1982).
30. S. Diamond, Proc. Conf. (Cem. and Concr. Assn.), pp. 2–30 (1976).